Research Article

Zhen Yang, Zheng Zhang, Peng Cheng, Zhe Long, Qi Cheng, Jiaqi Yang, Yu Lin, Bin Fang, Zhongming Zeng, Zhiping Zhou, Ganapathy Senthil Murugan* and Rongping Wang*

Monolithic temperature-insensitive high-Q Ta$_2$O$_5$ microdisk resonator

Abstract: We demonstrate a temperature-insensitive high-Q tantalum oxide (Ta$_2$O$_5$) microdisk resonator fabricated using electron-beam lithography and inductively coupled plasma reactive-ion etching. The microdisks exhibit a loaded Q-factor of 4.25×10^5 at 1,550 nm, which more than doubles ($\sim 9.3 \times 10^5$) following thermal annealing at 600 °C. Remarkably, the temperature-dependent resonant wavelength shift is suppressed to less than 10 pm/°C across a broad 100 nm bandwidth. Furthermore, the resonators maintain high optical stability under elevated input powers, with no observed degradation in optical properties such as extinction ratio or Q-factor. The combination of high Q-factors and exceptional thermal stability positions the Ta$_2$O$_5$ microdisk resonators as a promising platform for integrated photonic device applications, including on-chip narrow-linewidth lasers and precision sensing.

Keywords: tantala waveguide; microdisk resonator; optical cavity

---

*Corresponding authors: Rongping Wang, Laboratory of Infrared Materia and Devices, Advanced Technology Research Institute, Ningbo University, Ningbo, Zhejiang, 315211, China,
E-mail: wangrongping@nbu.edu.cn.
https://orcid.org/0000-0002-4426-824X; and **Ganapathy Senthil Murugan**, Optoelectronics Research Centre, University of Southampton, Southampton, SO17 1BJ, United Kingdom, E-mail: smg@orc.soton.ac.uk
Zhen Yang, Laboratory of Infrared Materia and Devices, Advanced Technology Research Institute, Ningbo University, Ningbo, Zhejiang, 315211, China; and Nanofabrication Facility, Suzhou Institute of Nano-Tech and Nano-Bionics, Chinese Academy of Sciences, Suzhou, 215123, China
Zheng Zhang, Peng Cheng, Zhe Long, Qi Cheng and Jiaqi Yang, Laboratory of Infrared Materia and Devices, Advanced Technology Research Institute, Ningbo University, Ningbo, Zhejiang, 315211, China
Yu Lin, Bin Fang and Zhongming Zeng, Nanofabrication Facility, Suzhou Institute of Nano-Tech and Nano-Bionics, Chinese Academy of Sciences, Suzhou, 215123, China
Zhiping Zhou, State Key Laboratory of Advanced Optical Communications Systems and Networks, School of Electrics, Peking University, Beijing, 100871, China

1 Introduction

Optical microresonators with high-quality factors (high-Q) and low optical losses are fundamental building blocks for diverse integrated photonic applications [1], [2], including nonlinear optics [3], precision biochemical sensing [4], and on-chip lasers [5]. These microcavities extend the photon lifetimes and tightly confine lightwaves within small volumes, significantly enhancing the intensity of the optical resonance fields. This enhancement improves device performance and enables novel photonic functionalities [6]. Recent advances have demonstrated high-Q microcavities on numerous material platforms, such as silicon (Si) [7], silicon nitride (Si$_3$N$_4$) [8], tantalum oxide (Ta$_2$O$_5$) [9], lithium niobate/tantalate (LiNbO$_3$/LiTaO$_3$) [3], [10]–[12], silicon carbide (SiC) [13], and III-V semiconductors [14]. However, the resonant wavelengths of high-Q microresonators are highly sensitive to environmental temperature fluctuations. This instability poses a critical challenge for applications requiring temperature-independent operation, such as dense wavelength division multiplexing (DWDM) systems and frequency-stabilized microlasers. A key limitation lies in the difficulty of simultaneously achieving both high-Q factors and thermal stability in existing microresonators. In previously reported adiabatic microcavity devices, materials with negative thermo-optic coefficients are used as cladding, and the waveguide size is reduced to expand the effective interaction area between the light field in the waveguide core and the negative thermo-optic coefficient material, enabling adiabatic operation across the entire waveguide. However, these approaches typically yield large mode volumes and Q factors on the order of 10^4 [15]–[17], which significantly degrade performance in practical photonics devices. Especially for on-chip light source applications, achieving thermally stable operation on a single material platform with small mode volume (leading to a stronger interaction between the optical field and the material) without sacrificing the optical performance of the microcavity device is crucial, and further extensive research is still needed.

Among the numerous silicon-compatible materials in photonic research, Ta$_2$O$_5$ stands out as a promising material for integrated photonic devices due to its attractive features, including a wide transparency window spanning the ultraviolet to infrared (0.28–8 μm) [18], a high refractive index ($n_0 = 2.05$ at 1,550 nm) relative to SiO$_2$ [19], a relatively high nonlinear refractive index (7.2×10^{-19} m^2/W) [20] – approximately three times larger than that of silicon nitride – and a low thermo-optic coefficient (5.75×10^{-6}/K), which is two orders of magnitude smaller than that of silicon (1.34×10^{-4}/K) [21]. In addition, Ta$_2$O$_5$ allows straightforward and high-throughput deposition of high optical quality thin films onto diverse substrates at room temperature. To date, Ta$_2$O$_5$-based photonic devices have been applied in various fields, such as dielectric metasurface optics [22], nonlinear optics [9], and rare-earth ion doped waveguide amplifiers [23]. Although the thermal stability of Ta$_2$O$_5$ microring resonators has been characterized [21], [24], [25], the thermal stability performance of Ta$_2$O$_5$ microdisk cavities has not been reported.

In this paper, we report an athermal, high-Q Ta$_2$O$_5$ microdisk resonator fabricated using electron-beam lithography and inductively coupled plasma reactive ion etching. After annealing, the Q-factor of the Ta$_2$O$_5$ microdisk resonator reaches approximately 9.3×10^5. At the same time, thermal stability across a bandwidth of approximately 100 nm, along with high power-handling stability without degradation in optical performance, is achieved. Synchronized implementation of ultrahigh Q-factor and exceptional thermal stability in Ta$_2$O$_5$ microdisk is key novelty of this work, demonstrating the significant potential of Ta$_2$O$_5$ microdisk resonators for applications in telecommunications, quantum optics, and precision measurement, where the demand for stable, high-Q resonators continues to rise.

2 Device fabrication and measurement

The Ta$_2$O$_5$ microdisk resonator was fabricated as follows. A 400 nm-thick Ta$_2$O$_5$ film was deposited via ion beam sputtering (IBS) onto a 4-inch silicon wafer with a 2 μm-thick thermal oxide layer. The metallic Ta target was sputtered with an oxygen flow of 48 sccm and a sputtering power of 400 W in a home-made IBS system. The refractive index dispersion of the deposited film was characterized using a Woollam V-VASE32 ellipsometer and is plotted in Figure 1(a). The surface roughness of the Ta$_2$O$_5$ film, measured using a Bruker Dimension ICON atomic force microscope (AFM), was determined to be R$_q$ (RMS) = 0.08 nm, as shown in Figure 1(b).

Figure 2(a) illustrates the fabrication process of the Ta$_2$O$_5$ microdisk resonator. Initially, an 80 nm-thick chromium (Cr) was deposited on the surface of the Ta$_2$O$_5$ film, serving as a hard mask. Subsequently, the devices were patterned with a 150 nm-thick hydrogen silsesquioxane (HSQ) photoresist using electron beam lithography (RAITH e-LINE Plus). The device structure was transferred to the Cr film through etching with a mixture of Cl$_2$ and O$_2$ gases. The underlying Ta$_2$O$_5$ layer was then fully etched using a low-pressure mixture of O$_2$, Ar and CF$_4$ gases in an inductively coupled plasma reactive ion etching (ICP-RIE) system (ULVAC NE-550). After etching, the device surface was treated with 400 W oxygen plasma for 10 min to remove the etching byproducts, and the Cr hard mask was subsequently removed using a chromium etchant (CR7T).

Figure 2(b) shows a scanning electron microscope (SEM) image of the fabricated microdisk resonator with a radius of 150 μm. The resonators are coupled to an access waveguide to enable optical characterization through transmission measurements. The magnified view of the coupling region, highlighted by the red frame in Figure 2(b) is shown in Figure 2(c). Figure 2(d) presents the cross-sectional SEM
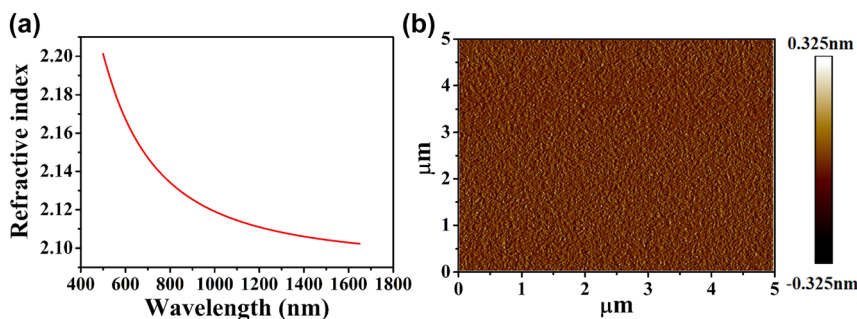

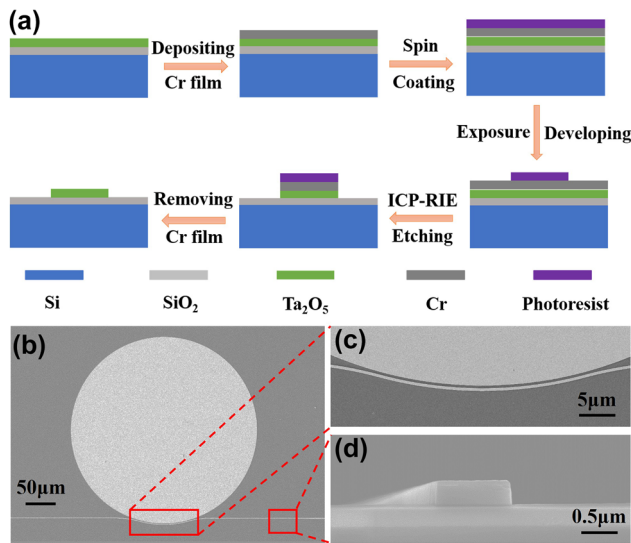**Figure 1:** (a) The measured refractive index, and (b) an AFM image of the deposited Ta$_2$O$_5$ film.

Figure 2: (a) Schematic illustration of the fabrication process flow.
(b) SEM image of a Ta$_2$O$_5$ microdisk resonator with a radius of 150 μm
and pulley-type coupler. (c) Magnified SEM image of the coupling region
highlighted in (b), showing the evanescent coupling gap between
the waveguide and microdisk. (d) Cross-sectional SEM image of
a fabricated Ta$_2$O$_5$ waveguide, with a width of 1,000 nm and a height
of 400 nm.

of a fabricated Ta$_2$O$_5$ waveguide. The waveguide has a width
(w) = 1,000 nm, a height (h) = 400 nm, and sidewall angles
(θ) = 89°. Evidently, the sidewalls are vertical and smooth,
demonstrating the high quality of the fabrication process.

In the experiments, light with a sub-MHz linewidth
from a tunable laser (Santac TSL-550) was coupled into the
bus waveguide end facet via a lensed fiber (SMF28e). On
the output side of the waveguide, the transmitted light was
collected and directed into a low-noise power meter (San-
tec MPM210) using a single-mode fiber (SMF). The coupled
optical power was maintained at a low level (~100 μW) to
minimize both nonlinear and thermo-optic effects within
the Ta$_2$O$_5$ waveguide. The polarization of the input light
was adjusted using a manual fiber polarization controller
(Thorlabs FPC526) to excite the fundamental quasi-TE mode
of the waveguide. To prevent any thermal drift of the res-
onator modes, the experimental temperature was fixed at
25 °C using a thermoelectric controller.

3 Results and discussion

Figure 3(a) shows the representative transmission spectrum
of the fabricated Ta$_2$O$_5$ microdisk resonator (radius: 150 μm)
measured at room temperature (25 °C). The power of the
coupled light was maintained at a low level (~100 μW) to

minimize any nonlinear effects. The microdisk resonator
operated in an under-coupled region with a 490 nm cou-
pling gap. Since the input laser coupled to microdisk res-
onator was adjusted to TE polarization, the resonant mode
in the transmission spectrum of the microdisk is primar-
ily dominated by TE modes, with no significant TM modes
observed. The Ta$_2$O$_5$ microdisk in this study has a radius of
150 μm and led to the excitation of high-order TE modes. By
analyzing the transmission spectrum, we identify the most
prominent resonant peaks as TE$_0$, TE$_1$, TE$_2$, and TE$_3$ modes,
with corresponding free spectral ranges (FSRs) of 1.2 nm,
1.18 nm, 1.17 nm, and 1.1 nm, respectively. These results are
shown in Figure 3(a). The representative resonant peak at
1,548.471 nm for the TE$_0$ mode was fitted with a Lorentzian
model as shown in Figure 3(b), yielding a full width at half
maximum (FWHM, denoted as $\Delta\lambda$) of 3.6 pm. Using the
relation $Q = \lambda/\Delta\lambda$, the loaded Q factor (Q_L) was calculated
as $\sim 4.25 \times 10^5$ at this wavelength. The intrinsic Q-factor
(Q_i) was determined to be 6.78×10^5 by using the equation
$Q_i = 2Q_L/\left(1 + \sqrt{T_0}\right)$ [19] for under-coupled devices, where
T_0 (=0.065) is the transmission normalized to the minimum
value of the fitting curves at the resonant wavelength.

Figure 3(c) shows the Q_L extracted from all reso-
nances of the TE fundamental mode between 1,500 nm and
1,600 nm. It was found that Q_L-values distribute at around
$\sim 3.5 \times 10^5$ in the investigated wavelength range. To the best
of our knowledge, this is the first demonstration of high-Q
Ta$_2$O$_5$ microdisks with bus waveguide coupling fabricated
via electron beam lithography (EBL) and inductively cou-
pled plasma reactive ion etching (ICP-RIE) – in contrast
to previously reported high-Q Ta$_2$O$_5$ microdisks fabricated
using photolithography-assisted chemical mechanical pol-
ishing and coupled via a tapered fibers [19]. To investi-
gate the impact of waveguide sidewall roughness and inter-
nal film stress/defects on optical losses, the Ta$_2$O$_5$ micro-
cavities were annealed at 600 °C for 10 h. As shown in
Figure 3(d), the Q_L increased significantly to $\sim 9.3 \times 10^5$ in
the annealed devices, and the intrinsic Q was calculated to
be 1.8×10^6. With annealing, the microdisk coupling state
gradually shifted towards a critical coupling state. Conse-
quently, the extinction ratio (ER) increased after annealing.
Further reduction in optical losses may be achieved by opti-
mizing the ICP-RIE etching parameters and improving the
coupling conditions between microdisk and the bus waveg-
uide. Alternatively, single-mode operation and enhanced Q-
factors could be realized by employing Euler-bent waveg-
uide designs to suppress higher-order modes and scattering
losses.

Thermo-optic properties play a critical role in stabiliz-
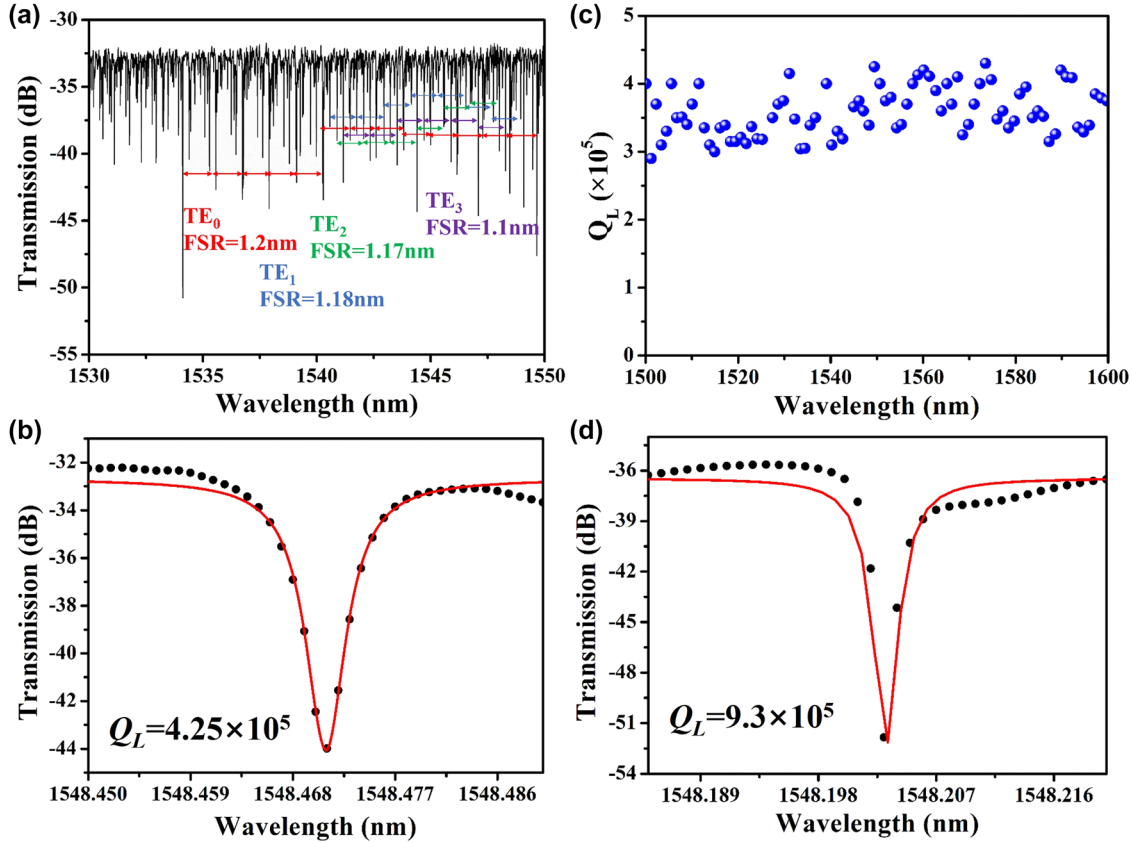ing on-chip light sources, particularly in applications such

Figure 3: (a) Measured transmission spectrum for the Ta$_2$O$_5$ microdisk resonator with radius = 150 µm and gap = 490 nm. (b) Measured spectrum (black dots) and Lorentzian fitting (red line) around the resonant wavelength at 1,548.471 nm. (c) Extracted Q_L (blue dot) at each resonant wavelength. (d) Measured Q factor of microdisk resonance wavelength at 1,548.2 nm after 600 °C annealing.

as microcavity-based soliton frequency combs [26] and rare-earth-doped laser systems [27]. To evaluate the thermo-optic response of Ta$_2$O$_5$ waveguides in the telecommunications band, temperature-dependent TE mode spectral measurements were performed on a Ta$_2$O$_5$ microdisk resonator. The substrate temperature was varied from 35 °C to 60 °C in 5 °C increments, covering multiple resonant wavelengths. Figure 4(a)-(c) display the linear dependence of the resonant wavelength on temperature at 1,505 nm, 1,550 nm, and 1,595 nm, yielding the resonance wavelength shifts ($d\lambda/dT$) of 8.99 pm/°C, 9 pm/°C, and 8.93 pm/°C, respectively. Figure 4(d) shows the resonant wavelength shift per °C across the entire telecom band, revealing a temperature-dependent shift of less than 10 pm/°C over a ~100 nm spectral bandwidth.

Table 1 compares the thermal stability of reported athermal microcavities across different material platforms. Microcavities based on materials with high thermo-optic coefficients, such as silicon and lithium niobate, typically require precise geometric engineering and the use of cladding layers with negative thermo-optic coefficients to

achieve athermal behaviour. However, these compensatory approaches often compromise optical performance, particularly the achievable Q-factors. In contrast, Ta$_2$O$_5$ offers intrinsic thermal stability due to its naturally low thermo-optic coefficient, enabling broadband athermal behaviour in microdisk resonators while preserving high quality (Q) factors (>10^5). This eliminates the need for complex structural modifications or performance trade-offs.

The temperature dependent wavelength shift ($\Delta\lambda$) of Ta$_2$O$_5$ microdisk resonator arises from both the thermal expansion effects and the thermo-optic effects according to Eq. (1) [35]

$$\Delta\lambda = \frac{d\lambda}{dT} = \lambda\left(\frac{1}{n_{\text{eff}}}\frac{dn_{\text{eff}}}{dT} + \frac{1}{R}\frac{dR}{dT}\right) \quad (1)$$

where $\frac{dn_{\text{eff}}}{dT}$ is the effective thermo-optic coefficient, $\frac{1}{R}\frac{dR}{dT}$ is the effective thermal expansion coefficient. However, due to silica's low thermal expansion coefficient and the thin Ta$_2$O$_5$ layer in our resonator geometry, material thermal expansion contributions are negligible [17]. From the measured wavelength shift of ~9 pm/°C at 1,550 nm, we calculated
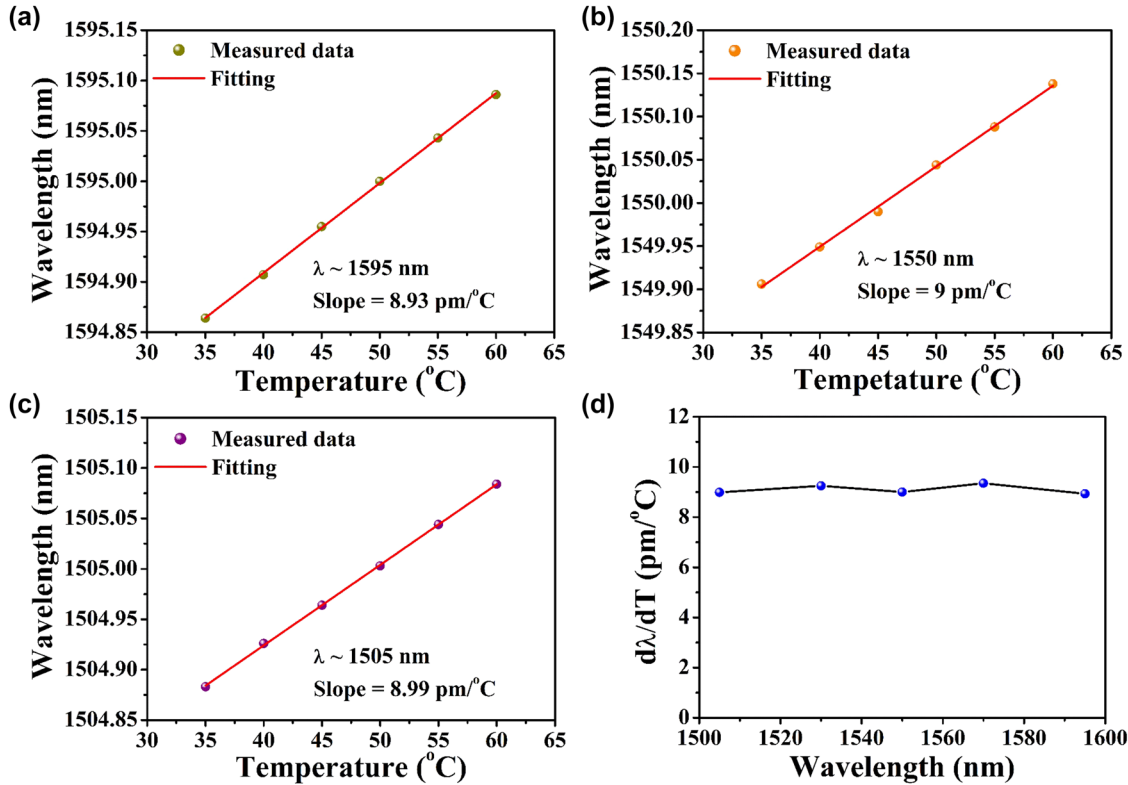
Figure 4: (a)–(c) Fitting of resonance wavelength with increasing temperature at various wavelength ranges around (a) 1,505 nm, (b) 1,550 nm, and (c) 1,595 nm. (d) Resonant wavelength shifts per °C across the entire telecom band.

Table 1: Comparison of reported parameters of athermal microcavities based on different material platforms.

Material	Cladding	Structure	dλ/dT (pm/K)	λ(nm)	Q_L	Athermal bandwidth (nm)	FOM[a] ($|Q_L/\Delta\lambda|$)	Ref.
Si	PSQ-LN	Ring	5	1,525	–	–	–	[28]
Si	LFR-372	Ring	0.2	1,550	1.8×10^4	–	9×10^4	[29]
Si	TiO$_2$	Ring	6.0	1,310	–	70	–	[30]
Si	TiO$_2$	Ring	−1.6	1,548	1.65×10^4	–	1.03×10^4	[15]
Si	EP	Ring	0.5	1,524	–	65	–	[31]
Si	Electro-optic polymer	Ring	2.1	1,550	1.25×10^4	–	0.6×10^4	[32]
Si	As$_{20}$S$_{80}$	Ring	13.95	1,610	2.6×10^5	80	1.86×10^4	[33]
Ta$_2$O$_5$	Air	Ring	7.8	1,543	5.5×10^4	–	0.71×10^4	[34]
Ta$_2$O$_5$	SiO$_2$	Ring	10.96	1,550	2.29×10^5	–	2.65×10^4	[25]
Ta$_2$O$_5$	Air	Ring	~9	1,549	1.84×10^6	–	20.4×10^4	[24]
Ta$_2$O$_5$	Air	Disk	9	1,550	9.3×10^5	100	10.3×10^4	**This work**
Ta$_2$O$_5$	SU-8	Disk	3	1,550	3.2×10^5	–	10.7×10^4	**This work**

[a]Higher is better.

a thermo-optic coefficient (TOC) of $\sim 4.8 \times 10^{-6}$/K for the Ta$_2$O$_5$ microdisk resonator, which is two orders of magnitude smaller than that of silicon, in excellent agreement with the published values [34], [35].

Since the focus of this study is to simultaneously achieve a high Q-factor and low thermal drift, we define a figure of merit (FOM) to compare the performance of our Ta$_2$O$_5$ resonator with other on-chip cavities. For a fair

comparison, we define the FOM given as FOM = $|Q_L/\Delta\lambda|$, which represents the ratio of the microcavity's load quality factor to the temperature-dependent wavelength shift. In the equation, Q_L represents the microcavity's load quality factor, and $\Delta\lambda$ represents the temperature-dependent wavelength shift. This FOM does not consider the resonator design and only compares the microcavity's quality factor and thermo-optical properties across different waveguides.
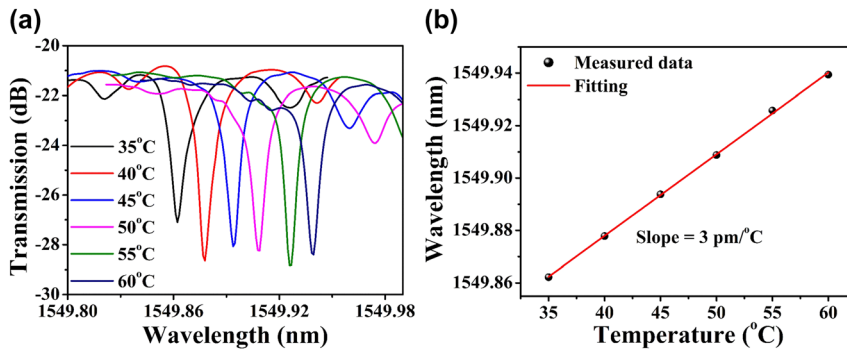
Figure 5: (a) Measured transmission spectra of the Ta$_2$O$_5$ microdisk resonator at various temperatures with SU-8 cladding, (b) the microdisk resonance wavelength shift with SU-8 cladding as a function of temperature.

A higher FOM is preferred, implying a higher quality factor and thermal stability of the microcavity. Table 1 summarizes a few representative designs with respect to this FOM.

To further enhance the thermal stability of the Ta$_2$O$_5$ microdisk, a 1 μm-thick SU-8 polymer layer was spin-coated onto the device to serve as an upper cladding. The SU-8 polymer, which possesses a negative thermo-optic coefficient (-2.9×10^{-4}/K) [35], was employed to partially compensate for the positive thermo-optic effect of the Ta$_2$O$_5$ microdisk. The resonance shift of the microdisk was characterized over a temperature range from 35 °C to 60 °C. As shown in Figure 5(a), the resonance peak at 1,549.8622 nm wavelength was red-shifted to 1,549.9394 nm. Figure 5(b) shows the linear relationship between resonant wavelength and temperature, with a fitted temperature sensitivity of approximately 3 pm/ °C, in contrast to the previous 9 pm/ °C, confirming that SU-8 upper cladding layer significantly improves thermal stability of the device. However, the improvement is limited. Due to the fixed geometry of the microdisk, the majority of the optical mode remains confined within the Ta$_2$O$_5$ core, and only a small portion interacts with the SU-8 cladding. As a result, the influence of SU-8's negative thermo-optic coefficient on the overall device stability is modest. The measured Q-factor of the SU-8–coated microdisk is approximately 3.2×10^5, lower than that of the air-clad counterpart. This reduction is likely due to unoptimized structural parameters, including cladding thickness, coupling coefficient, and microdisk radius. Here, we mainly characterize the thermal stability of the microdisk working in TE mode, and the thermal stability performance of the microdisk working in TM mode can be further tested later. The TE mode has a higher light field confinement capability than the TM mode, resulting in more light being confined to the Ta$_2$O$_5$ waveguide core and less light leaking into the SU-8 cladding. Conversely, for the TM mode, more light leaks into the SU-8 cladding. Therefore, under the same

external temperature and input power, Ta$_2$O$_5$ microdisks operating in the TM mode will exhibit superior thermal stability. Future work should focus on engineering the mode confinement to balance the optical field overlap between materials with positive and negative thermo-optic coefficients through carefully designing the SU-8 cladding thickness and the microdisk's radius and height. By integrating careful microcavity design with optimized fabrication processes, it will be possible to realize high-Q microresonators operating in the athermal regime, thereby enhancing their suitability for applications such as on-chip optical frequency comb generation.

In addition to the previously discussed characteristics, we further investigated the impact of high optical power on the stability of the Ta$_2$O$_5$ microcavity. Specifically, when the microcavity operates at its resonance wavelength, constructive interference leads to a buildup of intracavity power. In such cases, any linear or nonlinear absorption within the resonator can induce localized heating, which in turn may affect the optical properties of the device. Certain material platforms, such as Si [16] and SiC [36], are known to exhibit significant linear and nonlinear absorption under high-power operation, potentially degrading device performance. To evaluate whether similar effects occur in the Ta$_2$O$_5$ microdisk resonator, we used a tunable laser source to perform wavelength scans while monitoring the corresponding transmission spectra.

Figure 6(a) presents the power-dependent transmission spectra of the Ta$_2$O$_5$ microdisk resonator for coupled input powers ranging from 0.1 mW to 25.1 mW, the latter being limited by the maximum output power of the laser. Notably, the transmission spectra appear nearly identical across all input power levels. The corresponding resonant wavelengths under varying power conditions, extracted from Figure 6(a), are plotted and fitted in Figure 6(b). The results show that the resonance peak position remains virtually
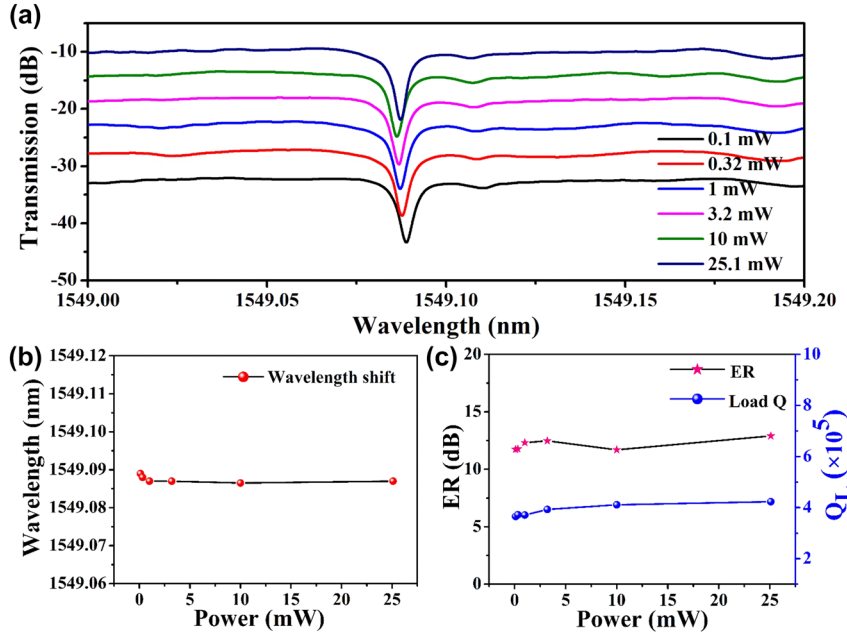
(a)

Figure 6: (a) Power-dependent transmission spectra of Ta$_2$O$_5$ microdisk resonator. (b) Extraction of the resonance peak position at different input power in (a). (c) Changes in the extinction ratio (ER) and loaded Q (Q_L) of the resonance peak at ~ 1,549.09 nm in (a) at various input powers.

unchanged as input power increases. In addition, the Q factors and extinction ratios (ER) associated with each resonance peak were extracted and are shown in Figure 6(c). The analysis indicates that neither the Q-factor nor the ER is significantly affected by increasing optical power. The Q-factors are consistently maintained around ~4×10^5, and the ER remains approximately 13 dB. The energy buildup in the Ta$_2$O$_5$ microdisk cavity primarily results from the field enhancement factor (FE). The field enhancement factor describes the ability of the cavity to amplify the local electric field amplitude. The power enhancement factor (M) describes the enhancement factor of the optical power stored or circulating within the cavity relative to the incident optical power. Because optical power is proportional to the square of the electric field intensity, the power enhancement factor is numerically equal to the square of the field enhancement factor [37]. At the resonance wavelength, the buildup factor can be estimated by [37], [38]:

$$\text{FE} = \left| \frac{\kappa}{1 - \tau \, \exp\left(\alpha L/2 + j\kappa L\right)} \right| \quad (2)$$

where a is the round-trip amplitude transmission, κ and τ are coupling coefficient and transmission coefficient, respectively. They are assumed to satisfy $\kappa^2 + \tau^2 = 1$, and can be calculated using equation $T_0 = (a - \tau)^2/(1 - a\tau)^2$, here T_0 is the fraction of transmitted optical power at the resonance wavelength. L is physical length of the microdisk resonator. Based on this, the field enhancement factor in

the Ta$_2$O$_5$ microdisk cavity is estimated to be approximately 22, indicating that the intracavity power at resonance is amplified by a factor of 484 compared to the input power. This observed stability confirms that Ta$_2$O$_5$ microcavities exhibit exceptional thermal insensitivity and negligible nonlinear absorption, even under conditions of high intracavity energy. These properties make Ta$_2$O$_5$ a highly promising material platform for developing thermally stable, high-performance on-chip integrated light sources.

4 Conclusions

In summary, we have demonstrated a high-Q, athermal Ta$_2$O$_5$ microdisk resonator fabricated using e-beam lithography and inductively coupled plasma reactive ion etching. The fabricated microdisk resonator with a radius of 150 μm exhibits a loaded Q-factor of 4.25×10^5 for the TE fundamental mode at 1,550 nm. After thermal annealing, the loaded Q-factor more than doubles, reaching approximately 9.3×10^5, with an intrinsic Q-factor as high as 1.8×10^6. Notably, the temperature-dependent resonant wavelength shift of the Ta$_2$O$_5$ microdisk remains below 10 pm/°C across the entire telecom band, spanning a ~100 nm bandwidth. Furthermore, power-dependent transmission measurements reveal no observable shift or distortion in resonant wavelengths, Q-factors (4×10^5), or extinction ratios (~13 dB), even at input powers up to 25.1 mW. These results confirm the

exceptional thermal insensitivity and low nonlinear absorption of Ta$_2$O$_5$ microdisks under high intracavity power conditions. The combination of ultrahigh Q-factors and superior thermal stability establishes Ta$_2$O$_5$ as a highly promising material platform for integrated, narrow-linewidth on-chip lasers [35]. Future work will focus on optimizing thermal compensation techniques, refining fabrication processes, and integrating these microresonators into scalable photonic circuits. This study represents a significant step forward realizing thermally robust, high-Q photonic devices, enabling new opportunities in precision metrology, quantum optics and integrated photonic systems.

Author contribution: ZY: data curation (lead); investigation (lead); writing – original draft (equal). ZheZ: data curation (supporting); investigation (supporting). PC: data curation (equal); investigation (supporting). ZL: data curation (supporting); investigation (supporting). QC: formal analysis (equal); supervision (equal); validation (equal). JY: investigation (supporting). YL: formal analysis (equal); supervision (equal); validation (equal). BF: formal analysis (equal); supervision (equal); validation (equal). ZhoZ: formal analysis (equal); supervision (equal); validation (equal). ZhiZ: formal analysis (equal); supervision (equal); validation (equal). GSM: conceptualization (lead); funding acquisition (lead); writing – review & editing (lead). RW: conceptualization (lead); formal analysis (equal); funding acquisition (lead); investigation (equal); project administration (lead); supervision (lead); validation (lead); writing – original draft (equal); writing – review & editing (lead). All authors have accepted responsibility for the entire content of this manuscript and consented to its submission to the journal, reviewed all the results and approved the final version of the manuscript.
Conflict of interest: Authors state no conflicts of interest.
Data availability: Data underlying the results presented in this paper are not publicly available at this time but may be obtained from the authors upon reasonable request.

References

[1] K. J. Vahala, "Optical microcavities," *Nature*, vol. 424, no. 6950, pp. 839−846, 2003.

[2] T. M. Benson *et al*., "Micro-optical resonators for microlasers and integrated optoelectronics," in *Frontiers in Planar Lightwave Circuit Technology: Design, Simulation, and Fabrication*, Berlin, Germany, Springer, 2006, pp. 39−70.

[3] C. Wang *et al*., "Lithium tantalate photonic integrated circuits for volume manufacturing," *Nature*, vols. 1−7, no. 8013, pp. 784−790, 2024.

[4] L. Zhang and D. Dai, "Silicon subwavelength-grating microdisks for optical sensing," *IEEE Photon. Technol. Lett.*, vol. 31, no. 15, pp. 1209−1212, 2019.

[5] W. Jin *et al*., "Hertz-linewidth semiconductor lasers using CMOS-ready ultra-high-Q microresonators," *Nat. Photonics*, vol. 15, no. 5, pp. 346−353, 2021.

[6] A. Matsko *et al*., "Review of applications of whispering-gallery mode resonators in photonics and nonlinear optics," *IPN Prog. Rep.*, vol. 42, no. 162, pp. 1−51, 2005.

[7] L. Zhang *et al*., "Ultrahigh-Q silicon racetrack resonators," *Photon. Res.*, vol. 8, no. 5, pp. 684−689, 2020.

[8] M. W. Puckett *et al*., "422 million intrinsic quality factor planar integrated all-waveguide resonator with sub-MHz linewidth," *Nat. Commun.*, vol. 12, no. 1, p. 934, 2021.

[9] H. Jung, S.-P. Yu, D. R. Carlson, T. E. Drake, T. C. Briles, and S. B. Papp, "Tantala Kerr nonlinear integrated photonics," *Optica*, vol. 8, no. 6, pp. 811−817, 2021.

[10] R. Gao *et al*., "Lithium niobate microring with ultra-high Q factor above 10^ 8," *Chin. Opt. Lett.*, vol. 20, no. 1, p. 011902, 2022.

[11] C. Li *et al*., "Ultra-high Q lithium niobate microring monolithically fabricated by photolithography assisted chemo-mechanical etching," *Opt. Express*, vol. 31, no. 19, pp. 31556−31562, 2023.

[12] M. Zhang, C. Wang, R. Cheng, A. Shams-Ansari, and M. Lončar, "Monolithic ultra-high-Q lithium niobate microring resonator," *Optica*, vol. 4, no. 12, pp. 1536−1537, 2017.

[13] C. Wang *et al*., "High-Q microresonators on 4H-silicon-carbide-on-insulator platform for nonlinear photonics," *Light Sci. Appl.*, vol. 10, no. 1, p. 139, 2021.

[14] W. Xie *et al*., "Ultrahigh-Q AlGaAs-on-insulator microresonators for integrated nonlinear photonics," *Opt. Express*, vol. 28, no. 22, pp. 32894−32906, 2020.

[15] S. S. Djordjevic *et al*., "CMOS-compatible, athermal silicon ring modulators clad with titanium dioxide," *Opt. Express*, vol. 21, no. 12, pp. 13958−13968, 2013.

[16] S. Grillanda *et al*., "Post-fabrication trimming of athermal silicon waveguides," *Opt. Lett.*, vol. 38, no. 24, pp. 5450−5453, 2013.

[17] G. Kang *et al*., "High quality chalcogenide-silica hybrid wedge resonator," *Opt. Express*, vol. 25, no. 13, pp. 15581−15589, 2017.

[18] M. Belt, M. L. Davenport, J. E. Bowers, and D. J. Blumenthal, "Ultra-low-loss Ta$_2$O$_5$-core/SiO$_2$-clad planar waveguides on Si substrates," *Optica*, vol. 4, no. 5, pp. 532−536, 2017.

[19] M. Li *et al*., "Fabrication of ultra-high-Q Ta$_2$O$_5$ microdisks by photolithography-assisted chemo-mechanical etching," *Opt. Express*, vol. 32, no. 17, pp. 29566−29572, 2024.

[20] C.-Y. Tai *et al*., "Determination of nonlinear refractive index in a Ta$_2$O$_5$ rib waveguide using self-phase modulation," *Opt. Express*, vol. 12, no. 21, pp. 5110−5116, 2004.

[21] C.-L. Wu *et al*., "Tantalum pentoxide (Ta$_2$O$_5$) based athermal micro-ring resonator," *OSA Continuum*, vol. 2, no. 4, pp. 1198−1206, 2019.

[22] C. Zhang *et al*., "Tantalum pentoxide: A new material platform for high-performance dielectric metasurface optics in the ultraviolet and visible region," *Light Sci. Appl.*, vol. 13, no. 1, p. 23, 2024.

[23] Z. Zhang *et al*., "On-chip Er-doped Ta$_2$O$_5$ waveguide amplifiers with a high internal net gain," *Opt. Lett.*, vol. 48, no. 21, pp. 5799−5802, 2023.

[24] J. Rasmus Bankwitz *et al*., "High-quality factor Ta$_2$O$_5$-on-insulator resonators with ultimate thermal stability," *Opt. Lett.*, vol. 48, no. 21, pp. 5783−5786, 2023.

[25] Q. Zhao *et al*., "Low-loss low thermo-optic coefficient Ta$_2$O$_5$ on crystal quartz planar optical waveguides," *APL Photonics*, vol. 5, no. 11, p. 116103, 2020.

[26] D. Xia *et al*., "Integrated chalcogenide photonics for microresonator soliton combs," *Laser Photon. Rev.*, vol. 17, no. 3, p. 2370013, 2023.

[27] K. Miarabbas Kiani, H. C. Frankis, C. M. Naraine, D. B. Bonneville, A. P. Knights, and J. D. B. Bradley, "Lasing in a hybrid rare-earth silicon microdisk," *Laser Photon. Rev.*, vol. 16, no. 1, p. 2100348, 2022.

[28] J. Teng *et al*., "Athermal Silicon-on-insulator ring resonators by overlaying a polymer cladding on narrowed waveguides," *Opt. Express*, vol. 17, no. 17, pp. 14627−14633, 2009.

[29] M. M. Milošević, N. G. Emerson, F. Y. Gardes, X. Chen, A. A. D. T. Adikaari, and G. Z. Mashanovich, "Athermal waveguides for optical communication wavelengths," *Opt. Lett.*, vol. 36, no. 23, pp. 4659−4661, 2011.

[30] S. Feng *et al*., "Athermal silicon ring resonators clad with titanium dioxide for 1.3 μm wavelength operation," *Opt. Express*, vol. 23, no. 20, pp. 25653−25660, 2015.

[31] V. Raghunathan, N. Y. Winnie, J. Hu, T. Izuhara, J. Michel, and L. Kimerling, "Athermal operation of silicon waveguides: Spectral, second order and footprint dependencies," *Opt. Express*, vol. 18, no. 17, pp. 17631−17639, 2010.

[32] F. Qiu *et al*., "Athermal hybrid silicon/polymer ring resonator electro-optic modulator," *Acs Photonics*, vol. 3, no. 5, pp. 780−783, 2016.

[33] P. Jean, A. Douaud, T. Thibault, S. LaRochelle, Y. Messaddeq, and W. Shi, "Sulfur-rich chalcogenide claddings for athermal and high-q silicon microring resonators," *Opt. Mater. Express*, vol. 11, no. 3, pp. 913−925, 2021.

[34] J. Ling, Y. He, R. Luo, H. Liang, and Q. Lin, "Athermal lithium niobate microresonator," *Opt. Express*, vol. 28, no. 15, pp. 21682−21691, 2020.

[35] Z. Geng *et al*., "Low-loss tantalum pentoxide photonics with a CMOS-compatible process," *Opt. Express*, vol. 32, no. 7, pp. 12291−12302, 2024.

[36] P. Xing, D. Ma, L. C. Kimerling, A. M. Agarwal, and D. T. H. Tan, "High efficiency four wave mixing and optical bistability in amorphous silicon carbide ring resonators," *APL Photonics*, vol. 5, no. 7, p. 076110, 2020.

[37] Y. Zheng, M. Pu, A. Yi, X. Ou, and H. Ou, "4H-SiC microring resonators for nonlinear integrated photonics," *Opt. Lett.*, vol. 44, no. 23, pp. 5784−5787, 2019.

[38] W. Bogaerts *et al*., "Silicon microring resonators," *Laser Photon. Rev.*, vol. 6, no. 1, pp. 47−73, 2012.